Oxygen tolerance of an *in silico*-designed bioinspired hydrogen-evolving catalyst in water

Patrick H.-L. Sit[a,1], Roberto Car[a,b], Morrel H. Cohen[a,c], and Annabella Selloni[a]

[a]Department of Chemistry and [b]Princeton Institute for the Science and Technology of Materials, Princeton University, Princeton, NJ 08544; and [c]Department of Physics and Astronomy, Rutgers University, Piscataway, NJ 08854

Edited by Michael L. Klein, Temple University, Philadelphia, PA, and approved December 19, 2012 (received for review September 4, 2012)

Certain bacterial enzymes, the diiron hydrogenases, have turnover numbers for hydrogen production from water as large as 10^4/s. Their much smaller common active site, composed of earth-abundant materials, has a structure that is an attractive starting point for the design of a practical catalyst for electrocatalytic or solar photocatalytic hydrogen production from water. In earlier work, our group has reported the computational design of $[FeFe]_P/FeS_2$, a hydrogenase-inspired catalyst/electrode complex, which is efficient and stable throughout the production cycle. However, the diiron hydrogenases are highly sensitive to ambient oxygen by a mechanism not yet understood in detail. An issue critical for practical use of $[FeFe]_P/FeS_2$ is whether this catalyst/electrode complex is tolerant to the ambient oxygen. We report demonstration by ab initio simulations that the complex is indeed tolerant to dissolved oxygen over timescales long enough for practical application, reducing it efficiently. This promising hydrogen-producing catalyst, composed of earth-abundant materials and with a diffusion-limited rate in acidified water, is efficient as well as oxygen tolerant.

energy storage | renewable energy | density functional theory | Car–Parrinello molecular dynamics

Photo- or electrocatalytic production of hydrogen from water has attracted much attention, prompting efforts to design a catalyst composed of earth-abundant elements. Insight into the design of such a catalyst can be gained from nature as, e.g., the diiron hydrogenases of certain anaerobic bacteria produce hydrogen efficiently (1–5). In particular, that of *Desulfovibrio desulfuricans* has a turnover number approaching 10^4/s (6). The high reactivity of the diiron hydrogenases suggests using a model of their common active site (Fig. 1) to start theoretical design of a practical catalyst for photo- or electrocatalytic production of hydrogen from water (7, 8).

Recently, we designed (7–9) a stable, efficient electrocatalyst, the $[FeFe]_P$ cluster (Fig. 2), for H_2 production starting from the diiron hydrogenase active center. The cluster, attached directly to an FeS_2 (100) surface, forms an $[FeFe]_P/FeS_2$ catalyst/electrode complex, reaching a density of reactive sites two orders of magnitude higher than obtainable by attaching the enzyme to the surface. The direct link between the active center and the surface accelerates electron transfer over that obtained by attaching the enzyme, within which the active center is buried.

The $[FeFe]_P$ catalyst could be an efficient, inexpensive hydrogen producer (8, 9) if it avoids the O_2 poisoning of the hydrogenase active center (*SI Appendix*) (5, 10–12). To address this, we have investigated the binding of solvated oxygen to $[FeFe]_P/FeS_2$ and its subsequent reaction with the cluster in water via density-functional theory calculations and Car–Parrinello molecular-dynamics simulations (13). [No consensus has emerged for the oxygen poisoning mechanism of the enzyme or of models of its active site from experiment (5, 10, 12, 14–19) or theory (20–25) (*SI Appendix*, section S1) to guide our analysis of the oxygen sensitivity of $[FeFe]_P/FeS_2$ beyond agreement that the oxidation process begins with an oxygen molecule binding to the distal iron, Fe_d, of the diiron cluster (Fig. 1*A*).] We find the cluster to be oxygen tolerant, reducing to water any oxygen it binds and surviving without structural change for times far longer than those of practical concern. To understand this tolerance, we carried out parallel studies of various O_2-sensitive unsupported model clusters. The poisoning mechanism we found, opening of the Fe-μC-Fe bridge bond by deletion of the μC, is frustrated by stabilization of that critical bond in $[FeFe]_P/FeS_2$.

Models

Fig. 1 shows relevant models of the diiron hydrogenase active site whereas Fig. 2 is a side view of the $[FeFe]_P$ cluster bound to the (100) surface of FeS_2. In the latter, the distal and the proximal irons, Fe_d and Fe_p, respectively, are bridged by a chelating $SCH_2CH_2CH_2P$ group. Fe_d is exposed to the water, and Fe_p is linked to the surface via an Fe-S bond. The C atom of a μCNH group bridges Fe_p and Fe_d. That group connects to an Fe atom of the FeS_2 (100) surface via a dative bond with its N atom. A third dative bond forms between another surface iron and the N atom of $(CHNH)_p$. The (100) FeS_2 electrode is modeled as a nine-layer film (8).

Reaction of O_2 with $[FeFe]_H$ and the H-Cluster in Vacuo

Ascertaining whether O_2 inactivates $[FeFe]_P$ in acidified water requires computationally intense Car–Parrinello simulations of the complex reactions between them. Insights into the mechanisms of O_2 poisoning or tolerance for simpler systems can help in planning the computations on $[FeFe]_P$ in acidified water and provide a basis for the interpretation of the results. We therefore first studied the reaction of O_2 with $[FeFe]_H$-related clusters, including the full H-cluster, and $[FeFe]_P$ in vacuo.

Binding of O_2 to $[FeFe]_H$ and the H-Cluster in Vacuo. O_2 binds to Fe_d end-on for all clusters studied. *SI Appendix*, Table S1 shows the binding energies, Fe_d-O and O-O distances, and the lowest-energy spin states of O_2 bound to $[FeFe]_H$ obtained for various charge states and terminating ligands L (Fig. 3, *Inset*), using the PBE functional (*Methods*). Structural changes upon O_2 binding were minor except for the cubane-containing H-cluster for which all CO ligands were terminally coordinated before O_2 binding and upon binding one moved from Fe_d into the bridge-bonding position (compare figures 5b and 6a of ref. 20). In studies of electron transfer in metal-dioxygen adducts on surfaces, the O_2-metal bond strength correlates directly with charge transfer and inversely with the ionization energy of the donor (26, 27). One expects such correlations here, provided no significant structural changes occur upon O_2 binding. The binding energies in *SI Appendix*, Table S1 do correlate inversely with the ionization energies of the $[FeFe]_H(L)$ clusters in various charge states, i.e., the straight line in Fig. 3, the least-squares fit to the points associated with no significant change of structure. Even the omitted point for the B3LYP TZ study of the H-cluster model fit shows a rough correlation. [Our results for the

Author contributions: P.H.-L.S., R.C., M.H.C., and A.S. designed research; P.H.-L.S. performed research; P.H.-L.S., R.C., M.H.C., and A.S. analyzed data; and P.H.-L.S. and M.H.C. wrote the paper.

The authors declare no conflict of interest.

This article is a PNAS Direct Submission.

[1]To whom correspondence should be addressed. E-mail: hsit@princeton.edu.

This article contains supporting information online at www.pnas.org/lookup/suppl/doi:10.1073/pnas.1215149110/-/DCSupplemental.

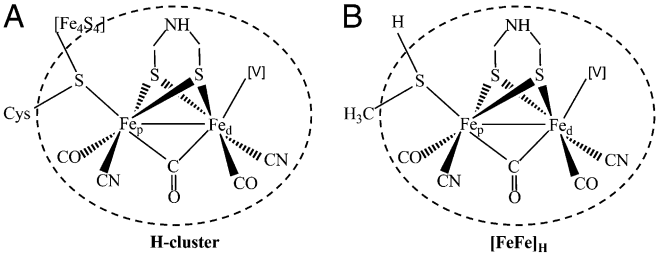

Fig. 1. Schematic structures of the H-cluster and the $[FeFe]_H$ cluster. (*A*) Structure of the H-cluster of the active site of the diiron hydrogenase enzyme of *Desulfovibrio desulfuricans*. It is composed of two subclusters, $[FeFe]_{Hs}$ and a cubane (Fe_4S_4), connected by a cysteine ligand. The dashed oval encloses the $[FeFe]_{Hs}$ subcluster. (*B*) Structure of the $[FeFe]_H$ cluster. The undercoordinated S of the $[FeFe]_{Hs}$ subcluster is replaced by a methanethiol. [V] symbolizes the vacant coordination site on Fe_d.

H-cluster are compared in *SI Appendix* with those of previous theoretical studies (20, 22).]

The values of the O-O separations in *SI Appendix*, Tables S1 and S3 indicate superoxide formation by transfer of an electron from the cluster to the oxygen. This is confirmed by relevant maximally localized Wannier densities (MLWD) and their centers of gravity (Wannier centers, WC) (*SI Appendix*, Fig. S1) (9, 28). The locations of the WC and the shapes of the MLWD indicate that the O_2-Fe_d link is a dative pair bond (*SI Appendix*, Fig. S1) (9, 28), with the superoxide as donor. According to the WC count (9, 28), the oxidation state (OS) was Fe(II)Fe(I) (Fe_d to the right) before O_2 binding. After binding it is Fe(II)Fe(II), implying electron transfer from Fe_d to the O_2.

Protonation of O_2-$[FeFe]_H$ and Poisoning of $[FeFe]_H$ in Vacuo. As in previous studies (20, 21), we find that the O-O bond breaks spontaneously after two protonations of the distal O, O_d, of the O_2-$[FeFe]_H^{-1}$ complex, releasing a water molecule. *SI Appendix*, Fig. S2*A* shows the optimized structure of the resulting cluster. Note that the Fe_d-μC bond has weakened.

We found three pathways for the reactions following O-O bond cleavage diagrammed in *SI Appendix*, Figs. S3–S5). In the first one (*SI Appendix*, Fig. S3), two protons and two electrons are transferred sequentially to O_p at Fe_d. The proton affinities exceed that of pure water, 295.5 kcal/mol, suggesting the transfers might be favorable in an aqueous environment. (Note that the proton affinity for a negatively charged system in vacuo may be larger than that in aqueous solution. Thus the fact that the proton affinity in vacuo exceeds that of pure water does not fully guarantee that spontaneous transfer from a solvated hydronium to a solvated cluster in the −1 charge state occurs.) The water molecule formed dissociates spontaneously, recovering the $[FeFe]_H^{-1}$ cluster. The oxygen is reduced to two water molecules.

The second pathway (*SI Appendix*, Fig. S4) deviates from the first one after release of the H_2O formed from O_d. O_p combines with a CO ligand on Fe_d, forming a CO_2 molecule that dissociates spontaneously as found in a previous study (20). The bridging site is opened (*SI Appendix*, Fig. S2*B*), by transition of the bridging CO to terminal coordination of Fe_d. Two protons and two electrons are then added sequentially; the protons bind at Fe_d. The two protonation energies exceed the proton affinity of water, suggesting that such proton transfers from water could be energetically favorable. The 1.74-Å distance between protons implies that two hydrides are bound separately to Fe_d as confirmed by MLWD analysis (*SI Appendix*, Fig. S6). Subsequent H_2 evolution is endoenergetic by only 1.3 kcal/mol, with a barrier of 4.8 kcal/mol. The small reaction energy and energy barrier imply that the modified cluster could still produce hydrogen, with entropy gain on desorption outweighing energy cost.

The third pathway (*SI Appendix*, Fig. S5) deviates from the second one after the formation of CO_2. Two protons and two electrons are added sequentially to the cluster. The first proton binds in the vacant Fe-Fe bridging position. This μH configuration is more stable by 15.1 kcal/mol than the terminal Fe_d-H configuration of the second pathway. After the first electron transfer, the second proton cannot bind to the μH but can bind to Fe_d. A hydrogen molecule can be formed after a second electron transfer by coordinated desorption of the two Hs from the bridging site and Fe_d. The H_2 desorption and barrier energies are 13.4 and 19.8 kcal/mol, respectively. Alternatively, a third proton can be stably bound to the still undercoordinated Fe_d after the second electron transfer. The energy of desorption of the resulting H_2 molecule from Fe_d is 19.9 kcal/mol; there is no barrier. These large energies imply that the third reaction pathway leads to inactivation of the cluster via exposure of the bridging site to proton binding by desorption of the CO_2. Therefore, the critical questions for us to answer are: Does an analogous reaction pathway exist for $[FeFe]_P$ in acidified water? And, if so, what is its lifetime against such a potentially deleterious structural change?

Reactions of $[FeFe]_p$ with O_2 in Vacuo

Structural optimizations and first-principles molecular dynamics simulations were performed in vacuo to identify reaction intermediates in the oxidation of $[FeFe]_P$, primarily in the −1 charge state it has at the initiation of H_2 production (8, 9).

O_2 Binding to $[FeFe]_p$ in Vacuo. After the pyrite Fe sites, Fe_d is the most favorable site for binding O_2. Table 1 shows formal OSs, binding energies, most stable spin states, and relevant structural data for the charge states −1, 0, and +1. O_2 does not bind to $[FeFe]_P$ in the charge state −1, as indicated by the large 3.64-Å separation and small (within our error) 0.2 kcal/mol endoenergicity in the stationary configuration. The formal OSs are those assigned to the Fe assuming the ligands are not redox active. The unit spin and the 1.24-Å O-O separation also indicate an unbound O_2 molecule.

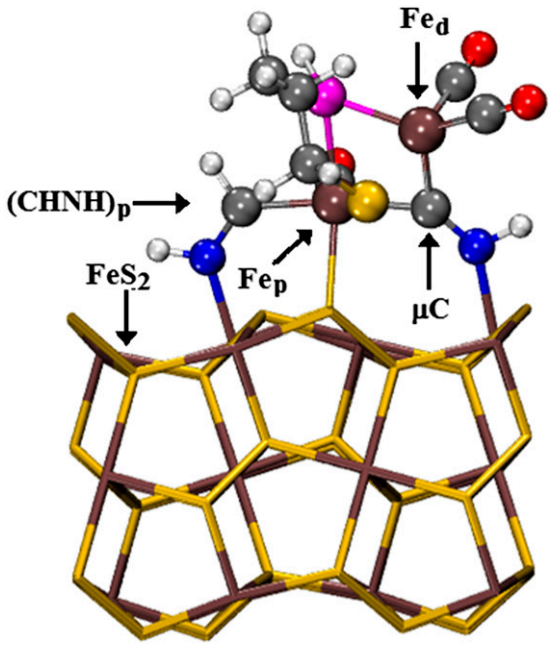

Fig. 2. Side view of the supported $[FeFe]_p$ catalyst. Key atoms and groups are indicated. The color convention throughout is Fe atoms, brown; S atoms, yellow; P atoms, violet; C atoms, gray; N atoms, blue; O atoms, red; and H atoms, white.

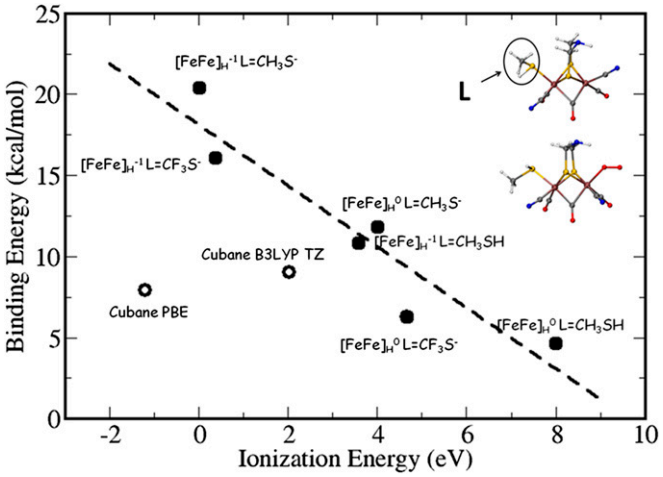

Fig. 3. Binding energy of O_2 vs. vertical ionization energy of $[FeFe]_H(L)$ clusters before binding. Solid circles represent clusters without significant structural changes on binding. The straight line is the least-squares fit to those points. Open circles represent the H-cluster for which significant structural change occurs. Unless stated otherwise, all calculations were performed with the PBE functional and a plane-wave basis (*Methods*). (*Upper Inset*) The $HSCH_3$ group of $[FeFe]_H$ within the oval is replaced by the various ligands L of *SI Appendix*, Table S1. (*Lower Inset*) The $[FeFe]_H$ cluster after O_2 binding.

In all charge states the O_2 binding energies of the $[FeFe]_P$ cluster are smaller than those of the $[FeFe]_H$ and H clusters, indicating a lower O_2 sensitivity of $[FeFe]_P$ in vacuo. For protonation of O_2-$[FeFe]_P^{-1}$ to occur and further reactions to proceed, O_p must be forced much closer to Fe_d. The relative stability of the $S = 0$, 1 states switches as O_p approaches Fe_d. The $S = 0$ state becomes less unstable than the $S = 1$ state by 8.0 kcal/mol at its local minimum. Thus, although O_2 is not bound to Fe_d in the most stable $S = 1$ state, there is a metastable binding configuration, O_2-$[FeFe]_P^{-1}$, in the $S = 0$ state, with an energy increase of +3.6 kcal/mol above the $S = 1$ nonbinding configuration and a barrier of +7.2 kcal/mol between them. See *SI Appendix*, Fig. S7 for both energy profiles.

There are several reasons why O_2 binding to $[FeFe]_H^{-1}$ is exothermic, although endothermic for $[FeFe]_P^{-1}$. First, the oxidation states differ, Fe(II)Fe(I) for $[FeFe]_H^{-1}$ vs. Fe(I)Fe(I) for $[FeFe]_P^{-1}$. In fact, Table 1 shows that O_2 binding becomes exothermic for $[FeFe]_P^{0}$, which has oxidation state Fe(II)Fe(I). Another important difference is the ligand composition of Fe_d, which has been recently discussed in detail by Stiebritz et al. (22). Following their work, we explored several mutations of the Fe_d ligands in $[FeFe]_P^{-1}$. We found that changing one of the two CO ligands to CN^-, as present in $[FeFe]_H^{-1}$, makes the binding of O_2 to $[FeFe]_P^{-1}$ exothermic by ~8 kcal/mol. Instead, other mutations, e.g., changing the PH group of $[FeFe]_P^{-1}$ to S, as present in $[FeFe]_H^{-1}$, have very little effect on O_2 binding. Finally, another important difference between $[FeFe]_P^{-1}$ and $[FeFe]_H^{-1}$ concerns the CNH vs. CO bridging ligand. However, modification of CNH in $[FeFe]_P^{-1}$ to CO opens the bridge. This damaging structural change makes the substitution irrelevant.

Table 1. Formal OS, binding energies (BE), spin states, and relevant structural data for O_2 binding to $[FeFe]_P$

Formal OS	Charge state	BE, kcal/mol	Spin, S	Fe_d-O, Å	O-O, Å
Fe(I)Fe(I)	−1	−0.2	1	3.64	1.24
Fe(II)Fe(I)	0	3.5	1/2	2.02	1.29
Fe(II)Fe(II)	+1	5.1	0	2.05	1.28
Fe(II)Fe(II)	+1	5.0	1	2.04	1.28

Negative values of BE indicate that the binding is endothermic. O_2 binds stably to Fe_d in charge states 0 and +1, not relevant to H_2 production. The spin 0 and 1 states are almost degenerate in the charge state +1.

Protonation of O_2-$[FeFe]_P^{-1}$ and Subsequent Recovery of $[FeFe]_P^{-1}$ in Vacuo. We studied the protonation and subsequent evolution of O_2-$[FeFe]_p^{-1}$ by total energy calculations. Fig. 4 shows the intermediates along the reaction pathway. In each protonation, a proton and an electron were added together to simulate the proton and electron transfer processes, maintaining a total charge of −1. The hydrogen addition energies are relative to half the energy of a hydrogen molecule. With the O_2-$[FeFe]_p^{-1}$ initially in the metastable $S = 0$ state, the first hydrogen binds to O_d with a favorable addition energy ΔE of −13.1 kcal/mol. The second hydrogen addition to O_d is more favorable with a ΔE of −85.4 kcal/mol. This large energy gain is related to the formation of a water molecule that desorbs spontaneously, removing O_d. O_p moves over to the nearby CO ligand and forms a CO_2 that stays ligated to the Fe_d. Desorption of this CO_2 ligand has an energy cost and barrier of 11.9 and 18.1 kcal/mol, respectively, in sharp contrast to the spontaneous desorption of the CO_2 formed on $[FeFe]_H$. We have also calculated the energy for the second protonation on O_p after O_d is singly protonated. It is less favorable by 65.4 kcal/mol than the case when O_d is doubly protonated.

A hydrogen added to the O_p of the ligated CO_2 binds with an energy cost of only +1.3 kcal/mol. The ligand becomes $COOH^-$; its desorption has a prohibitive energy cost of 58.9 kcal/mol. A second hydrogenation of O_p lowers the energy by 18.7 kcal/mol, forming a water molecule that spontaneously desorbs, carrying O_p away and restoring the $[FeFe]_P^{-1}$ cluster. It is the locking of $[FeFe]_P/FeS_2$ in the μCNH bridging configuration that makes desorption of the CO_2 unfavorable and opens a pathway to full O_2 reduction, suggesting that $[FeFe]_P$ might be oxygen tolerant in water as well. Thus, a pathway analogous to the second pathway for $[FeFe]_H$ exists for $[FeFe]_P$ in vacuo although, importantly, without bridge opening. So, if in water the free-energy barrier for CO_2 or $COOH^-$ dissociation were comparably large, O_2 tolerance would be possible.

Reactions in Water

Seventy-nine water molecules were added to simulate real neutral water. After equilibration, (undissociated) water molecules were adsorbed on each of the six Fe sites per unit cell not linked to the cluster. This is in principle a metastable equilibrium, as the simulated pH is much higher than the pH of zero charge, pH_{zpc} = 1.4, of FeS_2 (29). However, it is in practice the true equilibrium configuration, because the pH cannot be adjusted continuously in our simulations.

O_2 Binding to $[FeFe]_P$ in Water and First Protonation of O_d. Simulation of the oxidation of $[FeFe]_P^{-1}$ by molecular oxygen in water was initiated with the O_p of an added O_2 and Fe_d separated by 4.19 Å and the system in the $S = 1$ state. The O_2 moves away from Fe_d, staying at distances of 5.1–5.7 Å, implying a finite free-energy barrier to the initial oxidation step, as in vacuo. The separation of the O_p from Fe_d was reduced to 1.9 Å, and the spin changed to $S = 0$. Fig. 5 shows five representative snapshots taken from the ensuing simulation. The O_2 remains bound to Fe_d initially as a peroxide, as discussed in *SI Appendix*, section S9 and Fig. S9, but O_d abstracts a proton from a neighboring water molecule after 0.86 ps. The resulting OH^-, in the black circle in Fig. 5, moves via an H-bond chain to the pyrite surface where it takes up a proton from an adsorbed water molecule, becoming a water molecule by 1.35 ps and converting the latter into an adsorbed OH^-.

The free-energy profiles of O_2 binding and the two subsequent steps of the reaction illustrated in Fig. 5, the proton transfer from a water molecule to O_d and the OH^- transfer along the H-bond chain, are shown in *SI Appendix*, Fig. S8. The profiles were obtained from computationally demanding constrained Car–Parrinello

CHEMISTRY

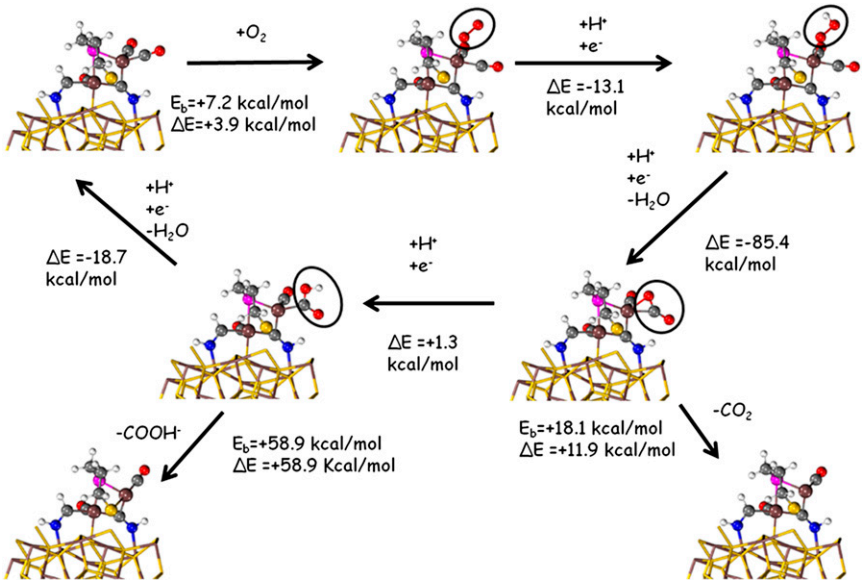

Fig. 4. $[FeFe]_P^{-1}$ recovery pathway in vacuo. Addition energies ΔE for H binding are relative to the energy of $1/2H_2$. E_b are the energy barriers.

molecular dynamics simulations. As in vacuo (*SI Appendix*, Fig. S7), the $S = 1$ state is energetically favored when O_2 is not bound to the Fe_d, whereas the $S = 0$ spin state is favored in the metastable binding configuration. The spin is unity in the O_2 adsorption free-energy calculations and zero in the two proton-transfer calculations. During the simulation of O_2 bound with $S = 0$, the average Fe_d-O_p distance is 1.93 Å. At that distance, the singlet state is energetically stabler by 2.2 kcal/mol in vacuo (*SI Appendix*, Fig. S7). Assuming the entropy to be insensitive to spin state apart from the contribution of multiplicity, we take 1.6 kcal/mol for the free-energy difference between the spin states at that separation and use it to align the first proton transfer profile with the O_2 absorption profile in *SI Appendix*, Figure S8.

The O_2-binding pathway has a free-energy barrier of 15.2 kcal/mol (*SI Appendix*, Fig. S8). This was obtained from calculations on the $S = 1$ surface, as suggested by the free-energy profiles in vacuo (*SI Appendix*, Fig. S7). It is unlikely that in water the switch

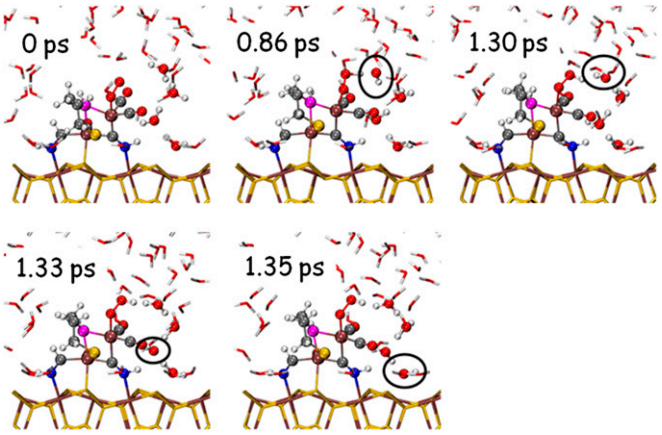

Fig. 5. Proton transfer from ambient water to O_2-Fe_d and migration of the resulting OH^-. Car–Parrinello molecular dyamics snapshots from a simulation with O_2 attached end-on to the Fe_d of the $[FeFe]_P^{-1}$ cluster solvated in neutral water. Only the catalyst and relevant waters are shown. At 0.86 ps the O_2 has abstracted a proton from the nearest water. The black ovals indicate the locations of the migrating hydroxide ion that then formed.

triplet→singlet occurs before the barrier on the triplet surface is reached, i.e., at distances larger than ∼2.2 Å (*SI Appendix*, Fig. S8). The solvation shell of O_2 in water has a radius of about 3.2 Å (30), so in the range of relevant Fe_d-O_p distances the influence of water on the Fe_d–O_2 interaction is expected to be negligible. (Results in ref. 30 have been checked and confirmed by our own Car–Parrinello molecular dynamics simulations for $^3O_2$ in bulk water.) The O_2-binding configuration is endothermic by 12.8 kcal/mol in the triplet state, reduced to 11.2 kcal/mol in the singlet state. The proton transfer from a water molecule to O_d is endothermic, but only by 1.2 kcal/mol, whereas the subsequent spontaneous OH^- transfer via the H-bond chain is highly exothermic. The overall free-energy reduction is 113.9 kcal/mol for the combined O_2 binding and first protonation of O_d. The pyrite surface apparently facilitates the protonation of O_d and stabilizes O_2 binding to Fe_d by providing a stable binding surface for hydroxide ions.

A proton was added to a water molecule in the bulk after the proton transfer from the surface water to O_d. That proton hopped rapidly to the surface OH^- via the Grotthuss mechanism to form a water molecule (*SI Appendix*, Fig. S10). This process parallels that of OH^-/hydronium recombination in bulk water reported in ref. 31. An added electron then restored the −1 charge of the cluster. However, had the added proton been already present during O_2 binding, it would most likely have migrated to the OH^- instead of the proton from the surface water. The surface OH^- would not have formed. The large free-energy release in *SI Appendix*, Fig. S8 is an artifact of our simulation, as discussed in *SI Appendix*, section S10.

Second Protonation of O_d in Water. Another proton added to a bulk water molecule closest to O_d (Fig. 6, black oval, 0 ps) spontaneously protonated it (black oval, 0.11 ps). The O-O bond of the dioxygen moiety then broke, and the water formed from O_d moved away (black oval, 0.18 ps). O_p then moved over to the CO ligand of Fe_d to form a CO_2 (Fig. 6, red oval, 0.38 ps) that remained ligated (Fig. 6, red oval, 1.43 ps), as in vacuo.

Protonations of O_p in Water; Recovery of the $[FeFe]_P^{-1}$ Cluster. After an electron was again added to restore the −1 charge, a proton was added to the water molecule (*SI Appendix*, Fig. S11, black oval) nearest O_p. Proton transfer to O_p created a $-COOH^-$ ligand, red oval, within 0.28 ps. An electron was added to the cluster, and

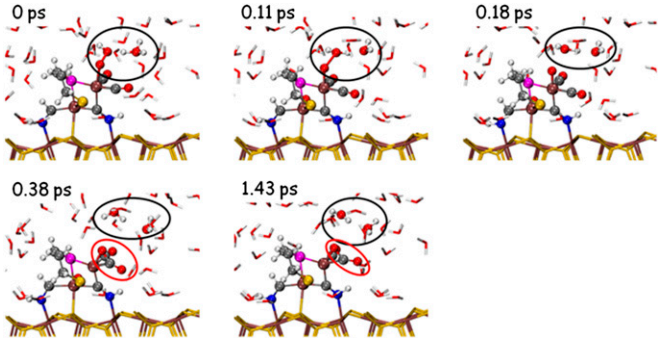

Fig. 6. Snapshots from the simulation of the second protonation of O_d. Only the catalyst and relevant waters are shown. See text for details.

a second proton was added to the water molecule nearest O_p (*SI Appendix*, Fig. S12), at 0 ps. Proton transfer to the O_p within the ligated $COOH^-$ had occurred spontaneously by 0.04 ps. The resulting water formed from O_p had desorbed from the CO ligand by 0.07 ps, restoring the $[FeFe]_P^{-1}$ cluster. Altogether, the attacking O_2 was reduced to two water molecules.

Conclusion: $[FeFe]_P$ Is Oxygen Tolerant

In earlier studies of H_2 production by $[FeFe]_H$ in vacuo and in water (32), we established that its CO-bridging configuration was essential and that its CO-terminal configuration, lower in energy in vacuo and competitive in water, bound protons too tightly at its open Fe-Fe bridging site. In the present study, we established that the attack of $[FeFe]_H$ by molecular oxygen leads to its poisoning by the opening of the bridging site to analogous tight proton binding. Although our primary motivation in redesigning $[FeFe]_H$ into $[FeFe]_P$ was to stabilize its structure and especially its bridging configuration in water during H_2 production, we now find that the changes made, particularly the stabilization of the bridging configuration, lead also to oxygen tolerance well in excess of any practical requirement.

Our simulations imply that permanent structural change of $[FeFe]_P^{-1}$ could proceed via two routes in acidified water. The first route is dissociation of the CO_2 on Fe_d formed by interaction of O_p with a CO ligand on Fe_d after O_d has been carried away as a water molecule, as shown in Fig. 4 for vacuum. The second is dissociation of $COOH^-$ after hydrogenation of the CO_2 before it dissociates (Fig. 4). In both cases the μC-bridging configuration would remain stable, leaving Fe_d undercoordinated. Two successive protonations of Fe_d and electron transfers, after an initial electron transfer to the cluster to restore the −1 charge state in the latter case, could either produce H_2 or result in a poisoned configuration in which the Hs are too tightly bound to produce H_2. However, we find via the kinetic analysis detailed in *SI Appendix* that such structural changes are sufficiently improbable to be irrelevant.

In *SI Appendix* we obtain and evaluate the following expression for the lifetime τ against structural change

$$1/\tau = 1/\tau_1 + 1/\tau_2 = \nu_{CO_2} e^{-\Delta F_b/kT}\left(e^{-\Delta F_1/kT} + e^{-\Delta F_2/kT}\right)[O_2],$$

where τ_1 is the lifetime against CO_2 desorption and τ_2 is that against $COOH^-$ dissociation. ΔF_b =11.2 kcal/mol is the free-energy difference between metastably bound and dissolved O_2 obtained from our and experimental data on O_2 in H_2O. ΔF_1 = 47.7 kcal/mol is the free-energy barrier for CO_2 dissociation computed by constrained Car–Parrinello molecular dynamics simulation. This barrier in water is significantly larger than that calculated in vacuo because the simulation shows that hydrogen bonds are broken in the dissociation process in water. ΔF_2 is the free-energy barrier for $COOH^-$ dissociation estimated to exceed the 58.9 kcal/mol dissociation energy in vacuo because of expected similarly broken water hydrogen bonds. $[O_2]$ is the bulk molecular fraction of O_2 (less than its saturation value of 0.464×10^{-5} at 25 °C), and ν_{CO2} is the attempt frequency for O_2 binding estimated to be kT/h ~ 10^{12}/s. We obtain a lower bound for τ of 3.2×10^{27} y at 25 °C. The catalyst is thus oxygen tolerant on any practical timescale, with ample margin for error in the computations and estimates.

The lifetime is so long because of the large positive values of the three ΔFs. The strong tridentate binding of the cluster to the pyrite surface can be expected to increase the ionization energy and thence ΔF_b according to the correlation in Fig. 3. Two effects contribute to the large values of ΔF_1 and ΔF_2. The first one is the stability of the bridging configuration. The μCNH cannot move over to the terminal configuration on Fe_d to reduce the cost of CO_2 or $COOH^-$ dissociation by reducing its undercoordination. The second one is the cost of disruption of the water's H-bond network as the dissociating molecule moves into the water.

On the basis of the computed recovery pathway in vacuo of Fig. 4, we have performed a simplified analysis of the oxygen reduction reaction (ORR) at $[FeFe]_P$ under electrochemical conditions, using the idealized scheme developed by Nørskov and coworkers (33). The effects of immersion in water do not substantially change the conclusions (33). The results of this analysis are summarized in *SI Appendix*, section S13. *SI Appendix*, Fig. S13 shows the energy diagram for the ORR at several potentials; the reference potential is that of the standard hydrogen electrode so that the chemical potential of added ($H^+ + e^-$) equals that of 1/2 H_2 at pH = 0 (33). $[FeFe]_P$ is uninteresting as a pure ORR catalyst (33, 34), requiring an overpotential of 1.3 V, but sufficiently active for O_2 tolerance. We used the same approach to construct an analogous energy diagram (*SI Appendix*, Fig. S14), for the hydrogen evolution reaction (HER) (35). The computed overpotential for the HER on $[FeFe]_P^{-1}$ (the active ready state) is 0.5 V. Under the working conditions for hydrogen evolution, the ORR is barrierless, i.e., $[FeFe]_P$ efficiently reduces those oxygen molecules that reach the vacant Fe_d site. The analysis in *SI Appendix* of the microkinetic details of both reactions shows that the ORR is significantly slower and does not interfere with the HER. In conclusion, $[FeFe]_P$ is composed of earth-abundant elements, it is stable in the presence of ambient oxygen, its overpotential of 0.5 V is comparable to that of Au(111) (35), and its HER microkinetics are limited by proton diffusion because of its low barrier to first protonation (8) as discussed in *SI Appendix*. Together these favorable features imply that $[FeFe]_P$ is a promising HER catalyst.

Methods

Density functional theory computations on the $[FeFe]_H$ cluster in vacuo were carried out with the PBE functional (36) and a plane-wave basis set as implemented in the Quantum-ESPRESSO (37) package. Cutoff energies were 30 and 240 Ryd for the wavefunctions and the augmented charge density, respectively. A cubic supercell of 15.9 Å and Γ point sampling were used. For the $[FeFe]_H$ in vacuo, we also performed calculations, using the B3LYP hybrid functional and Ahlrichs' valence triple-zeta (TZ) basis set with polarization (38) as implemented in the NWCHEM package (39).

The calculations on the $[FeFe]_P$ cluster in vacuo were carried out with the PBE functional and plane-wave basis sets with the same cutoffs. The pyrite (100) surface was modeled in a periodic slab geometry, using the experimental lattice parameter, 5.428 Å (40), situated in a tetragonal simulation box with a = 10.856 Å and c = 21.712 Å. (Our theoretical lattice constant is 5.404 Å, 0.4% shorter than the experimental value.) We considered a 2 × 2 supercell having the ideal termination of the bulk. The slab was nine atomic layers thick with 24 FeS_2 units. K-space was sampled at the Γ point.

For calculations in water, the $[FeFe]_P$ cluster was situated in a tetragonal simulation box with a =10.856 Å and c = 32.568 Å and we added 79 water molecules to simulate immersion of the supported cluster in water of real density. Car–Parrinello molecular-dynamics simulations were performed with the CP code of the Quantum-ESPRESSO package, and free energies along reaction pathways were obtained from constrained molecular-dynamics

CHEMISTRY

simulations (41). A fictitious electronic mass of 350 a.u. and a time step of 0.072 fs were used, and the temperature was set at 330 K. (The temperature was set slightly higher than room temperature to compensate for the known underestimation of diffusion in water simulations, using the Perdew–Burke–Ernzerhof (PBE) functional (42).) The total spin was maintained along each molecular-dynamics trajectory. Maximally localized Wannier functions (28) and their centers were obtained using the CP code of the Quantum-ESPRESSO package.

ACKNOWLEDGMENTS. We acknowledge computational resources from the Princeton Institute for Computational Science and Engineering (PICSciE) and the Office of Information Technology (OIT) High Performance Computing Center and Visualization Laboratory at Princeton University. This work was supported by the Department of Energy, Office of Basic Energy Sciences, Division of Materials Sciences and Engineering under Award DE-FG02-06ER-46344. We also used resources of the National Energy Research Scientific Computing Center, which is supported by the Office of Science of the US Department of Energy under Contract DE-AC02-05CH11231.

1. Tard C, et al. (2005) Synthesis of the H-cluster framework of iron-only hydrogenase. *Nature* 433(7026):610–613.
2. Peters JW, Lanzilotta WN, Lemon BJ, Seefeldt LC (1998) X-ray crystal structure of the Fe-only hydrogenase (CpI) from Clostridium pasteurianum to 1.8 angstrom resolution. *Science* 282(5395):1853–1858.
3. Siegbahn PEM, Tye JW, Hall MB (2007) Computational studies of [NiFe] and [FeFe] hydrogenases. *Chem Rev* 107(10):4414–4435.
4. Adams MW, Stiefel EI (2000) Organometallic iron: The key to biological hydrogen metabolism. *Curr Opin Chem Biol* 4(2):214–220.
5. Baffert C, et al. (2008) Hydrogen-activating enzymes: Activity does not correlate with oxygen sensitivity. *Angew Chem Int Ed Engl* 47(11):2052–2054.
6. Hatchikian EC, Forget N, Fernandez VM, Williams R, Cammack R (1992) Further characterization of the [Fe]-hydrogenase from Desulfovibrio desulfuricans ATCC 7757. *Eur J Biochem* 209(1):357–365.
7. Zipoli F, Car R, Cohen MH, Selloni A (2010) Theoretical design by first principles molecular dynamics of a bioinspired electrode-catalyst system for electrocatalytic hydrogen production from acidified water. *J Chem Theory Comput* 6(6):3490–3502.
8. Zipoli F, Car R, Cohen MH, Selloni A (2010) Simulation of electrocatalytic hydrogen production by a bioinspired catalyst anchored to a pyrite electrode. *J Am Chem Soc* 132(25):8593–8601.
9. Sit PHL, et al. (2011) Oxidation state changes and electron flow in enzymatic catalysis and electrocatalysis through Wannier-function analysis. *Chemistry* 17(43):12136–12143.
10. Vincent KA, et al. (2005) Electrochemical definitions of O_2 sensitivity and oxidative inactivation in hydrogenases. *J Am Chem Soc* 127(51):18179–18189.
11. Imlay JA (2006) Iron-sulphur clusters and the problem with oxygen. *Mol Microbiol* 59(4):1073–1082.
12. Stripp ST, et al. (2009) How oxygen attacks [FeFe] hydrogenases from photosynthetic organisms. *Proc Natl Acad Sci USA* 106(41):17331–17336.
13. Car R, Parrinello M (1985) Unified approach for molecular dynamics and density-functional theory. *Phys Rev Lett* 55(22):2471–2474.
14. Liu T, Li B, Singleton ML, Hall MB, Darensbourg MY (2009) Sulfur oxygenates of biomimetics of the diiron subsite of the [FeFe]-hydrogenase active site: Properties and oxygen damage repair possibilities. *J Am Chem Soc* 131(23):8296–8307.
15. Goldet G, et al. (2009) Electrochemical kinetic investigations of the reactions of [FeFe]-hydrogenases with carbon monoxide and oxygen: Comparing the importance of gas tunnels and active-site electronic/redox effects. *J Am Chem Soc* 131(41):14979–14989.
16. Darensbourg MY, Weigand W (2011) Sulfoxygenation of active site models of [NiFe] and [FeFe] hydrogenases - A commentary on possible chemical models of hydrogenase enzyme oxygen sensitivity. *Eur J Inorg Chem* 2011:994–1004.
17. Lambertz C, et al. (2011) O_2 reactions at the six-iron active site (H-cluster) in [FeFe]-hydrogenase. *J Biol Chem* 286(47):40614–40623.
18. Liebgott PP, et al. (2010) Relating diffusion along the substrate tunnel and oxygen sensitivity in hydrogenase. *Nat Chem Biol* 6(1):63–70.
19. Lautier T, et al. (2011) The quest for a functional substrate access tunnel in FeFe hydrogenase. *Faraday Discuss* 148:385–407, discussion 421–441.
20. Stiebritz MT, Reiher M (2009) Theoretical study of dioxygen induced inhibition of [FeFe]-hydrogenase. *Inorg Chem* 48(15):7127–7140.
21. Dogaru D, Motiu S, Gogonea V (2009) Inactivation of [FeFe]-hydrogenase by O_2. Thermodynamics and frontier molecular orbitals analyses. *Int J Quantum Chem* 109(4):876–889.
22. Stiebritz MT, Finkelmann AR, Reiher M (2011) Oxygen coordination to the active site of Hmd in relation to [FeFe] hydrogenase. *Eur J Inorg Chem* 2011:1163–1171.
23. Dogaru D, Motiu S, Gogonea V (2010) Residue mutations in [FeFe]-hydrogenase impedes O_2 binding: A QM/MM investigation. *Int J Quantum Chem* 110:1784–1792.
24. Bruska MK, Stiebritz MT, Reiher M (2011) Regioselectivity of H cluster oxidation. *J Am Chem Soc* 133(50):20588–20603.
25. Hong G, Pachter R (2012) Inhibition of biocatalysis in [Fe-Fe] hydrogenase by oxygen: Molecular dynamics and density functional theory calculations. *ACS Chem Biol* 7(7):1268–1275.
26. Lever ABP, Ozin GA, Gray HB (1980) Electron transfer in metal-dioxygen adducts. *Inorg Chem* 19:1823–1824.
27. Cramer CJ, Tolman WB, Theopold KH, Rheingold AL (2003) Variable character of O-O and M-O bonding in side-on (η^2)) 1:1 metal complexes of O_2. *Proc Natl Acad Sci USA* 100(7):3635–3640.
28. Marzari N, Vanderbilt D (1997) Maximally localized generalized Wannier functions for composite energy bands. *Phys Rev B* 56:12847–12865.
29. Xu Y, Schoonen MAA (2000) The absolute energy positions of conduction and valence bands of selected semiconducting minerals. *Am Mineral* 85:543–556.
30. Fois E, Gamba A, Redaelli C (1999) Hydrophobic effects: A computer simulation study of the temperature influence in dilute O_2 aqueous solutions. *J Chem Phys* 110:1025–1035.
31. Hassanali A, Prakash MK, Eshet H, Parrinello M (2011) On the recombination of hydronium and hydroxide ions in water. *Proc Natl Acad Sci USA* 108(51):20410–20415.
32. Zipoli F, Car R, Cohen MH, Selloni A (2009) Hydrogen production by the naked active site of the di-iron hydrogenases in water. *J Phys Chem B* 113(39):13096–13106.
33. Nørskov JK, et al. (2004) Origin of the overpotential for oxygen reduction at a fuel-cell cathode. *J Phys Chem B* 108:17886–17892.
34. Kjaergaard CH, Rossmeisl J, Nørskov JK (2010) Enzymatic versus inorganic oxygen reduction catalysts: Comparison of the energy levels in a free-energy scheme. *Inorg Chem* 49(8):3567–3572.
35. Nørskov JK, et al. (2005) Trends in the exchange current for hydrogen evolution. *J Electrochem Soc* 152:J23–J26.
36. Perdew JP, Burke K, Ernzerhof M (1996) Generalized gradient approximation made simple. *Phys Rev Lett* 77(18):3865–3868.
37. Giannozzi P, et al. (2009) QUANTUM ESPRESSO: A modular and open-source software project for quantum simulations of materials. *J Phys Condens Matter* 21(39):395502–395520.
38. Schafer A, Huber C, Ahlrichs R (1994) Fully optimized contracted Gaussian basis sets of triple zeta valence quality for atoms Li to Kr. *J Chem Phys* 100:5829–5835.
39. Kendall RA, et al. (2000) High performance computational chemistry: An overview of NWChem a distributed parallel application. *Comput Phys Commun* 128:260–283.
40. Finklea SL III, Cathey L, Amma EL (1976) Investigation of the bonding mechanism in pyrite using the Mossbauer effect and X-ray crystallography. *Acta Crystallogr A* 32:529–537.
41. Frenkel D, Smit B (2002) *Understanding Molecular Simulation: From Algorithms to Applications* (Academic, New York).
42. Grossman JC, Schwegler E, Draeger EW, Gygi F, Galli G (2004) Towards an assessment of the accuracy of density functional theory for first principles simulations of water. *J Chem Phys* 120(1):300–311.